Using particle shape to induce tilted and bistable liquid crystal anchoring

BARMES, F. and CLEAVER, D. J. <http://orcid.org/0000-0002-4278-0098>

Using particle shape to induce tilted and bistable liquid crystal anchoring

F. Barmes[1] and D.J. Cleaver[2]

[1]*Centre Européen de Calcul Atomique et Moléculaire, 46, Allée d'Italie, 69007 Lyon, France*
[2]*Materials and Engineering Research Institute, Sheffield Hallam University, Sheffield, S1 1WB, United Kingdom*

(Dated: November 17, 2004)

We use Monte Carlo simulations of hard Gaussian overlap (HGO) particles symmetrically confined in slab geometry to investigate the role of particle-substrate interactions on liquid crystalline anchoring. Despite the restriction here to purely steric interactions and smooth substrates, a range of behaviours are captured, including tilted anchoring and homeotropic-planar bistability. These macroscopic behaviours are all achieved through appropriate tuning of the microscopics of the HGO-substrate interaction, based upon non-additive descriptions for the HGO-substrate shape parameter.

PACS numbers: 61.30.-v, 64.70Md, 61.30.Cz, 68.08.-p

I. INTRODUCTION

The term *surface anchoring* refers to the means by which a preferred orientation (or set of orientations) is imposed on a liquid crystal by a confining substrate [1]. The mechanisms underlying surface anchoring are fundamental to the operation of virtually all liquid crystal display cells, since the field-off states utilised in such devices are usually surface-aligned [2, 3]. Indeed, surface anchoring is particularly important in the latest generation of bistable devices [4–6] in which the display cells possess two optically distinct surface-stabilised arrangements.

Experimental studies of liquid crystal anchoring (see Jérôme [1] for a review) have identified three classes of alignment characterised by α, the angle between the average director tilt and the substrate normal. These alignments are homeotropic, tilted and planar with, respectively, $\alpha = 0$, $0 < \alpha < \pi/2$ and $\alpha = \pi/2$. The anchoring properties of adsorbed liquid crystalline systems have also been the subject of several theoretical investigations performed, in the main, using mean field [7, 8] and density functional [9–11] approaches.

Despite this range of previous studies, molecular-level understanding of the mechanisms driving anchoring remains limited and the methods used to control surface anchoring in current devices are largely empirical. For instance, it has long been known that rubbed substrates can be used to create planar surface alignment [12], but the mechanisms underlying this result have been the subject of an extended debate [13]. If the surface is a polymer film, soft rubbing has the effect of aligning the polymer chains in the rubbing direction. This, in turn, aligns the liquid crystal molecules thus highlighting a chemical mechanism coupling the nematic director in the interfacial region with the polymer chain orientation [14, 15]. If, however, the substrate is scratched by the rubbing, creating a grooved surface, it has been argued that a steric mechanism can generate the same effect [16].

While treatments such as substrate rubbing offer surface pretilt and azimuthal control over the anchoring direction, they do not represent the only routes to controllable liquid crystal alignment. This has been illustrated by a series of computer simulation studies performed over the last decade, which have given direct insight into the relationship between molecular adsorption and liquid crystal anchoring. The most common arrangement found in such studies is planar anchoring; this has been found at flat substrates for hard-particle [17–20], Gay-Berne [21] and all-atom [22] models (though note that planar alignment of the adsorbed molecules does *not* always result in planar anchoring [23]). Homeotropic anchoring has been achieved using hard-particle systems employing non-additive wall-particle interactions at perfectly flat walls [11, 19, 20, 24, 25] and full interactions at walls with tethered flexible chains [25–27] and rigid rods [28]. While homeotropic anchoring has been seen in simulations of Gay-Berne particles confined by smooth substrates [21], and could certainly be forced using the well-depth anisotropy tuning approach employed in [29], the majority of such systems have yielded tilted alignments [30–33]. Up to now, the tilt observed in these systems has been ascribed to competition between the particle-particle and particle-wall attractive interactions. However, by investigating the equivalent hard-particle system, we show here that this tilt actually has an *entropic* origin. Tilted anchoring in hard-particle systems has previously been seen only when the substrates have been made rough through the tethering of chains [25–27] or rods [28]. Indeed, entropy-driven tilt of cylindrically symmetric particles at smooth walls has not, to our knowledge, been seen or even considered in any previous simulation or theoretical study.

In this study we extend previous work [20] on the anchoring behaviour of generic hard-particle liquid crystal models by studying the effect of changing the particle-substrate contact function. Specifically, we use Monte Carlo simulations to study the anchoring behaviour of hard Gaussian overlap (HGO) particles confined in a slab geometry using two particle-surface potentials - the HGO-sphere and HGO-surface potentials. As well as investigating the intrinsic anchoring properties of these two surfaces, we study their behaviours for varying degrees of substrate penetrability, in order to identify the conditions under which the stable anchoring condition

changes. This is done with the aim of developing and characterising a surface potential capable of exhibiting both homeotropic and planar anchoring alignments, i.e. bistable anchoring. A narrow region of bistability was identified in our previous work based on the simple hard needle-wall (HNW) surface potential [20] and found to be explained by the non-additive nature of this potential.

The remainder of this paper is organised as follows: in Section II we describe the HGO-sphere potential and its induced phase behaviour. Following this, in Section III we show equivalent work performed with the HGO-surface model. Finally, in Section IV, we present a discussion and the conclusions deduced from this work and propose some directions for future work.

II. THE HGO-SPHERE SURFACE POTENTIAL

In this Section, surface induced structural changes are studied using Monte Carlo simulations of rod-shaped particles that interact with one another through the HGO potential [34] and with the confining substrates via the HGO-sphere potential. The HGO model is a steric model in which the contact distance is the shape parameter determined by Berne and Pechukas [35] when they considered the overlap of two ellipsoidal Gaussians. Thus, the interaction potential $\mathcal{V}^{\mathrm{HGO}}$ between two particles i and j with respective orientations $\hat{\mathbf{u}}_i$ and $\hat{\mathbf{u}}_j$ and intermolecular vector $\mathbf{r}_{ij} = r_{ij}\hat{\mathbf{r}}_{ij}$ is defined as

$$\mathcal{V}^{\mathrm{HGO}} = \begin{cases} 0 & \text{if } r_{ij} \geq \sigma(\hat{\mathbf{u}}_i, \hat{\mathbf{u}}_j, \hat{\mathbf{r}}_{ij}) \\ \infty & \text{if } r_{ij} < \sigma(\hat{\mathbf{u}}_i, \hat{\mathbf{u}}_j, \hat{\mathbf{r}}_{ij}) \end{cases} \tag{1}$$

where $\sigma(\hat{\mathbf{u}}_i, \hat{\mathbf{u}}_j, \hat{\mathbf{r}}_{ij})$ is the contact distance, or shape parameter,

$$\sigma(\hat{\mathbf{u}}_i, \hat{\mathbf{u}}_j, \hat{\mathbf{r}}_{ij}) = \sigma_0 \left\{ 1 - \frac{1}{2}\chi \left[\frac{(\hat{\mathbf{r}}_{ij}\cdot\hat{\mathbf{u}}_i + \hat{\mathbf{r}}_{ij}\cdot\hat{\mathbf{u}}_j)^2}{1+\chi(\hat{\mathbf{u}}_i\cdot\hat{\mathbf{u}}_j)} + \frac{(\hat{\mathbf{r}}_{ij}\cdot\hat{\mathbf{u}}_i - \hat{\mathbf{r}}_{ij}\cdot\hat{\mathbf{u}}_j)^2}{1-\chi(\hat{\mathbf{u}}_i\cdot\hat{\mathbf{u}}_j)} \right] \right\}^{-\frac{1}{2}}. \tag{2}$$

Here σ_0, the particle width, sets the unit of distance for this model and the shape anisotropy parameter $\chi = (k^2-1)/(k^2+1)$, where $k = \sigma_\ell/\sigma_0$, is the particle length to breadth ratio.

The HGO model is the hard-particle equivalent of the much-studied Gay-Berne model [36]. The phase behaviour of the HGO model is density driven and fairly simple, comprising only two non-crystalline phases; isotropic and (for $k \gtrsim 3$) nematic fluids at, respectively, low and high number densities ρ^*. The isotropic-nematic phase-coexistence densities have been located for various particle elongations in a series of previous simulation studies [37–39]; for the most commonly used elongation of $k = 3$, the isotropic-nematic transition occurs at $\rho^* \approx 0.30$ with a slight system size dependence.

Although the HGO model was originally derived using geometrical considerations, an HGO particle cannot be represented by a fixed solid object. Rather, it is a mathematical abstraction of the interaction surface between two non-spherical particles [34]. For moderate elongations, however, the properties of HGO particles are similar to those of an the equivalent hard ellipsoid of revolution [34]. Simulation studies [39] have borne this out, showing that the equation of state of the HGO fluid is qualitatively equivalent to, but consistently displaced from, that of the hard ellipsoid fluid.

The shape parameter $\sigma(\hat{\mathbf{u}}_i, \hat{\mathbf{u}}_j, \hat{\mathbf{r}}_{ij})$ given by eqn.(2) has too low a symmetry to be appropriate for describing the interaction between an HGO particle and a featureless, planar substrate. However, a simple function with the appropriate symmetry *is* obtained in the limit that one of the particles is made spherical. For a sphere of diameter σ_j, the contact distance for this interaction is given by eqn.(4) of [35] :

$$\sigma^{\mathrm{HGO-sphere}}(\hat{\mathbf{u}}_i, \hat{\mathbf{r}}_{ij}) = \sqrt{\frac{\sigma_0^2 + \sigma_j^2}{2(1-\chi(\mathbf{u_i}\cdot\mathbf{r_{ij}})^2)}}. \tag{3}$$

In Refs. [30–33], this contact function was used as the basis for the particle-substrate interaction: the surface, as viewed by any particle, was taken to be represented by a sphere located in the surface plane but with the same x- and y-coordinates as those of the particle. In this Section, we adopt this same HGO-sphere approximation for the particle-substrate contact function. We also investigate the dependence of the system's anchoring on the penetrability of the substrate. This is achieved by mediating the interaction between each particle and the substrate using a second "inner" particle of breadth σ_0 and length $\sigma'_\ell \leq \sigma_\ell$. Thus, when the inner particle is made short, the HGO becomes able to embed its ends into the substrate. This results in an interaction

$$\mathcal{V}^{\mathrm{HGO-sphere}} = \begin{cases} 0 & \text{if } |z_i - z_0| \geq \sigma_w^{\mathrm{HGO-sphere}}(\hat{\mathbf{u}}_i) \\ \infty & \text{if } |z_i - z_0| < \sigma_w^{\mathrm{HGO-sphere}}(\hat{\mathbf{u}}_i) \end{cases} \tag{4}$$

between particle i and a substrate located at z_0, where

$$\sigma_w^{\mathrm{HGO-sphere}}(\hat{\mathbf{u}}_i) = \sigma_0 \left[(1 - \chi_S \cos^2\theta_i)^{-1/2} - \frac{1}{2} \right] \tag{5}$$

is a rewriting of eqn. (3) in terms of θ_i, the particle zenithal angle, subject to the imposition $\sigma_j = \sigma_0$ and a shift of the surface spheres by one particle radius so as to make the substrate surface coincide with z_0. $\chi_S = (k_S^2 - 1)/(k_S^2 + 1)$, k_S being the length to breadth ratio (σ'_ℓ/σ_0) of the inner ellipsoid. In the next Subsections, the consequences of changing this variable will be examined. Broadly, reducing k_S, and so increasing the degree of surface penetrability is expected to stabilise the homeotropic arrangement. Indeed, previous simulation studies [11, 20] have shown the homeotropic state to be stable for $k_S = 0$. At the other limit, it is established that hard rods at hard walls adopt planar alignment [18]. And

between the two lies the possibility of substrate-induced tilt.

A. Simulation results

The surface induced structural changes obtained using the HGO-sphere potential have been investigated by means of Monte Carlo computer simulations in the canonical ensemble. Systems of $N = 1000$ HGO particles with elongation $k = 3$ were confined in a slab geometry with fixed wall separation $L_z = 4k\sigma_0$, the walls being situated at $z_0 = \pm\frac{L_z}{2}$ and symmetric anchoring conditions imposed. Periodic boundary conditions were applied in the x- and y-directions. At the time of the computation, one individual run of half a million sweeps represented about 30 hours of computation time on a Compaq dec alpha workstation. With more recent processors (intel pentium IV with 3.0GHz clock speed) this can be reduced to 5 hours bringing the total time to compute an anchoring map down to 300 hours of CPU time. The relatively modest system size of $N = 1000$ has been used here in order to enable a comprehensive mapping of the relevant phase space to be achieved. From De Miguel's study of system size effects in 3d bulk systems of Gay-Berne particles [40], it is apparent that any N-dependence of bulk behaviour should be negligible for $N \geq \mathcal{O}(10^3)$. This conclusion does not transfer automatically to confined systems, however, since the surface extrapolation lengths can become comparable with the substrate-substrate separation [41]. For the systems studied here, in which the surface conditions were symmetrical, we have found that doubling the slab thickness (*i.e.* running with $N = 2000$ particles) does not have a significant effect on the anchoring behaviour observed. However, in equivalent simulations of hybrid anchored systems, in which the two surface extrapolation length regions can promote competing effects, we have found that the slab thickness becomes a significant simulation parameter; this is described in detail elsewhere [42]. Sequences of simulations were performed at constant number density ρ^* and decreasing k_S for several values of ρ^*; from these simulations, the surface induced structural changes were studied through computation of profiles for the number density $\rho^*_\ell(z)$, orientational order with respect to the substrate normal, $Q_{zz}(z)$, and slice averaged orientational order, $\langle P_2(z)\rangle$. Full descriptions relating to the computation of these observables are given elsewhere [20, 31].

In Figs. 1 and 2, we show typical observable profiles obtained at isotropic and nematic densities for systems with $k_S/k = 0$ and $k_S/k = 1.0$, respectively. At low density, the system with $k_S/k = 0.0$ shows strong surface adsorption peaks adjacent to each substrate with high orientational order perpendicular to the surfaces. As expected, the central 50% of the system is orientationally isotropic. At the nematic density, however, the positive $Q_{zz}(z)$ profile values effectively replicate those obtained for $\langle P_2(z)\rangle$, indicating uniform homeotropic anchoring.

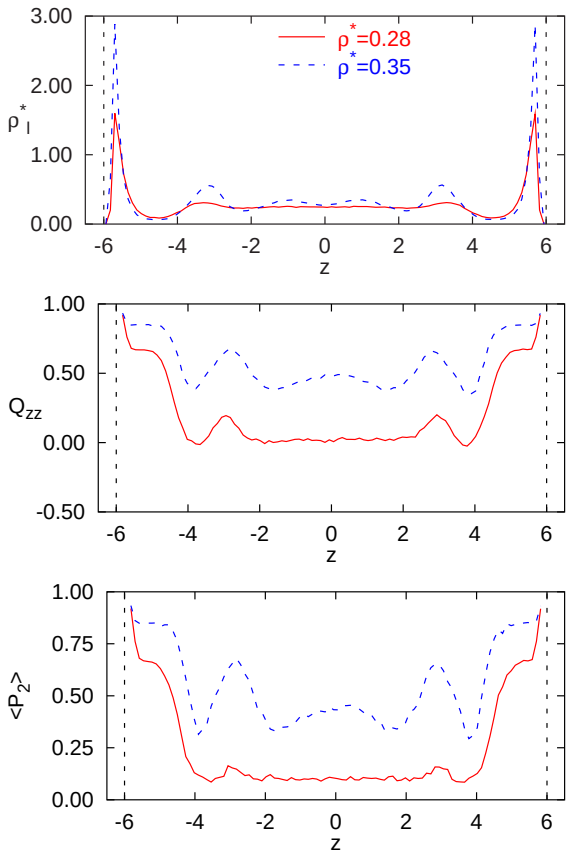

FIG. 1: [Color online] Typical z-profiles for confined systems of HGO particles with $k = 3.0$ and $k_S/k = 0.0$ using the HGO-sphere potential. These data are extracted from simulation series with decreasing k_S.

Furthermore, the peak separations of about σ_ℓ in the corresponding $\rho^*_\ell(z)$ profiles indicate substrate-templated pseudo-smectic layering of the type exhibited by other homeotropic systems [20, 31]. The equivalent profiles obtained from the $k_S/k = 1.0$ system indicate very different behaviour, however. At low densities, the surface density peaks are shifted away from the substrates, and no structure is apparent in $\rho^*_\ell(z)$ apart from these first-monolayer features. Additionally, this system has low order parameter throughout, with very little surface-enhancement compared with that shown by the homeotropic system. On compression to a nematic density, the $\rho^*_\ell(z)$ profile gains secondary peaks at each substrate, but the observed peak-peak separation distance is not appropriate for either homeotropic or planar anchoring states. Additionally, whilst the $\langle P_2(z)\rangle$ profile clearly indicates a well ordered nematic film at this density, the central region of the corresponding $Q_{zz}(z)$ profile adopts near-zero values. These features suggest a tilted arrangement, as is confirmed by the configuration snapshot, Fig. 3(b), generated for this system at $\rho^* = 0.35$.

The crossover from homeotropic to tilted anchoring has been studied further through extensive simulations per-

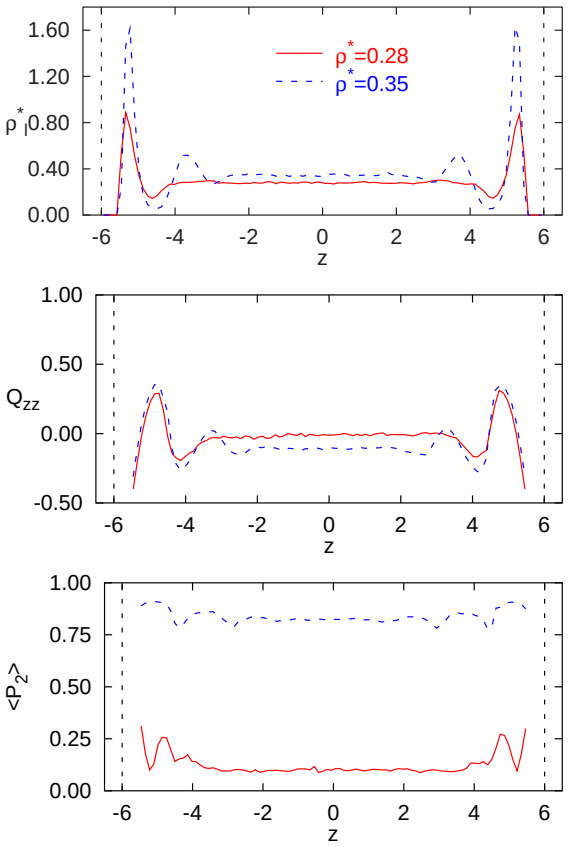

FIG. 2: [Color online] Typical z-profiles for confined systems of HGO particles with $k = 3.0$ and $k_S/k = 1.0$ using the HGO-sphere potential. These data are extracted from simulation series with decreasing k_S.

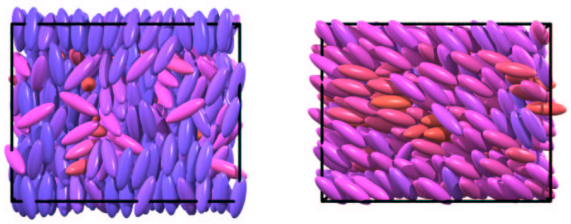

(a) $k_S/k = 0.0$ (b) $k_S/k = 1.0$

FIG. 3: [Color online] Typical configuration snapshots showing the surface induced (a) homeotropic ($k_S/k = 0$) and (b) tilted ($k_S/k = 1.0$) surface induced arrangements for confined systems of $N = 1000$ HGO particles using $\mathcal{V}^{\mathrm{HGO-sphere}}$ for surface interactions and $\rho^* = 0.35$.

formed over the $\rho^*, k_S/k$ phase space. These are summarised in the surface and bulk-region anchoring maps shown in Figs. 4 (a) and (b), respectively, and calculated following the method given in [20]. These maps show the contours of $\overline{Q_{zz}}(\rho^*, k_S/k)$, the density-profile-weighted average of $Q_{zz}(z)$ in the interfacial and bulk

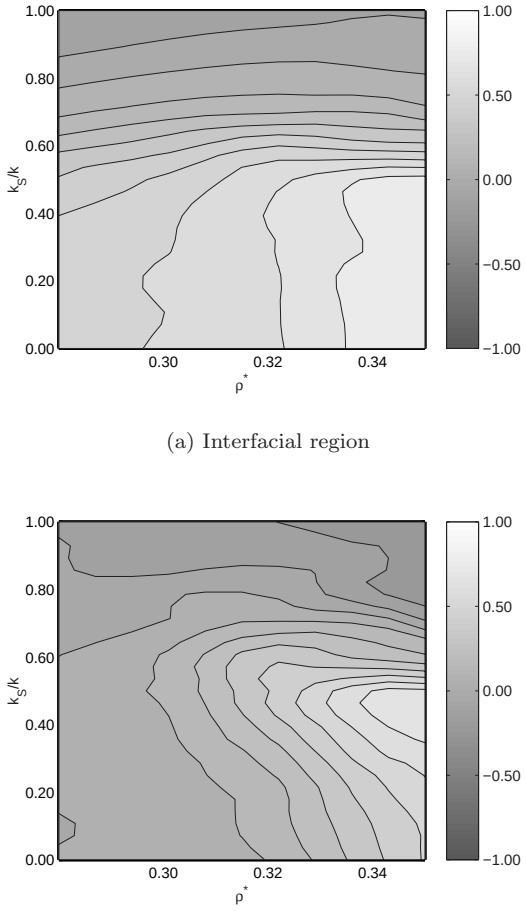

(a) Interfacial region

(b) Bulk region

FIG. 4: Anchoring maps showing the evolution of $\overline{Q_{zz}}(\rho^*, k_S/k)$ as obtained from series of simulations at constant density and decreasing k_S and using the HGO-sphere potential. Subfigures (a) and (b) correspond to the interfacial and bulk regions of the cell respectively.

regions of the cell. The difference between the computation of these profiles and those of [20] lies in the convention adopted to define the location of the boundary between the interfacial and bulk regions of the cell. Here, the interfacial region was taken to extend from the substrate to the second local maximum in $\rho^*_\ell(z)$ regardless of the surface arrangement. These maps indicate a transition between homeotropic and tilted anchoring states at $k_S/k \simeq 0.5$, but this crossover is less sharp than the homeotropic-planar anchoring transition observed with the HNW surface model [20]. Indeed, profiles obtained from simulation series performed at constant density but either increasing or decreasing k_S show negligible differences, indicating that the HGO-sphere model does not exhibit bistability for $k = 3$.

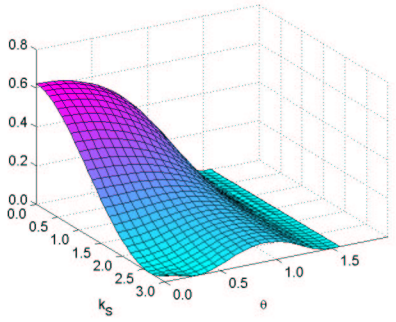

FIG. 5: [Color online] Representation of $V_{\rm abs}(k_S, \theta)$ for the HGO-sphere potential and $k = 3$.

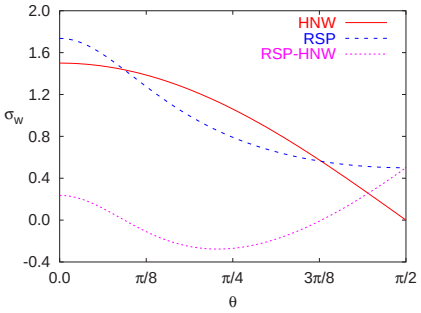

FIG. 6: [Color online] Comparison between $\sigma_w^{\rm HNW}$ (solid line) and $\sigma_w^{\rm HGO-sphere}$ (dashed line). The dotted line represents the difference between the two ($\sigma_w^{\rm HGO-sphere} - \sigma_w^{\rm HNW}$.)

B. Origin of the tilt

To examine the basis of the tilted anchoring identified in the previous Subsection, we now assess the geometrical properties of the HGO-sphere surface interaction model. As is shown in Appendix A, for an ellipsoid of elongation k and tilt θ whose closest surface-intersection-point lies a distance d from the ellipsoid centre, $V_{\rm abs}(k, \theta)$, the ellipsoid volume absorbed into the surface is given by :

$$V_{\rm abs}(k, d, \theta) = \frac{k\pi}{3}\left(\frac{1}{2} - \frac{d}{(k^2\cos^2\theta + \sin^2\theta)^{1/2}}\right)^2 \times \left(1 + \frac{d}{(k^2\cos^2\theta + \sin^2\theta)^{1/2}}\right). \quad (6)$$

Approximating this ellipsoid with the HGOs used in the simulations and d with $\sigma_w^{\rm HGO-sphere}(\hat{\mathbf{u}}_i)$ of eqn. (5), we obtain an expression for $V_{\rm abs}(k, k_S, \theta)$. Setting $k = 3$, we present in Fig. 5 a graphical representation of $V_{\rm abs}(k_S, \theta)$, the absorbed particle volume as a function of both k_S and θ. For short k_S, this adsorbed volume is maximal at $\theta = 0$, corresponding to an homeotropic anchoring state. As k_S approaches k, however, a second maximum develops at intermediate θ, which suggests the stability of a tilted arrangement.

More insight into this result can be gained by comparing the HGO-sphere shape parameter, eqn. (5), with that of the HNW potential, $\sigma_w^{\rm HNW} = 0.5 k_S \cos\theta$. In the case $k_S = k$, the latter represents the distance between the substrate and the particle's centre of mass when one of the particle's ends is in contact with the surface plane [20]. $\sigma_w^{\rm HGO-sphere}$, in contrast, represents the distance at which the HGO particle interacts with a sphere embedded within the substrate. The difference between the two shape parameters (Fig. 6) shows that, for intermediate tilt angles, $\sigma_w^{\rm HGO-sphere}$ drops below $\sigma_w^{\rm HNW}$. At these angles, therefore, the HGO-sphere surface potential allows the particle ends to penetrate the surface plane. The angles corresponding to this region of reduced $\sigma_w^{\rm HGO-sphere}$ coincide with the maximum in $V_{\rm abs}(k_S, \theta)$ and appear, therefore, to be associated with the tilt behaviour.

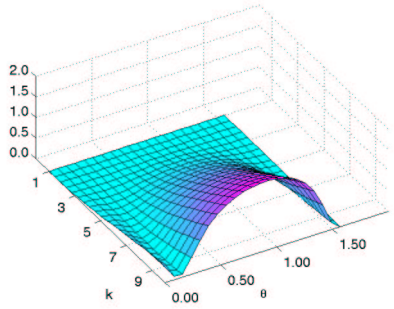

FIG. 7: [Color online] Representation of $V_{\rm abs}(k, \theta)$ for the HGO-sphere potential and $k_S = k$.

The tilt angle $\theta_{tilt}^{\rm max}$ for which the absorbed volume of a single particle is maximal can be calculated using eqn. (6) for various values of k and k_S. For example, we show (Fig. 7) the surface $V_{\rm abs}(k, \theta)$ calculated in the full-particle limit $k_S = k$. For this case, $\theta_{tilt}^{\rm max}(k)$ has been obtained by computing the contour of $\frac{d}{d\theta}V_{\rm abs}(k, \theta)$ at level 0, from which we have found that $\theta_{tilt}^{\rm max}$ is constant at about 0.9 radians ($\sim 50°$) for $k \leq 10$. This implies that a tilt angle of about 50° should be adopted by full (*i.e.* $k_S = k$) HGO particles adsorbed using the HGO-sphere potential. Despite both the neglect of many-body effects in this analysis and the geometrical approximations made, the prediction $\theta_{tilt}^{\rm max} \sim 50$ degrees matches the simulation results reasonably well. At the state point $\rho^* = 0.35$ and $k_S/k = 1.0$, for the z location where $\rho_\ell^*(z)$ is maximal, the simulations give $Q_{zz} = 0.209$, which corresponds to an average tilt angle of 46.6°. Since surface-packing of particles increases with decrease in tilt angle, the single-particle prediction for $\theta_{tilt}^{\rm max}$ can be expected to be an be an over-estimate; the tilt angle adopted in the simulations therefore appears to represent a reasonable compromise.

The numerical and geometrical treatments described in this Section have shown that a tilted phase can be both predicted and obtained with a purely steric model. This sheds new light on the tilted phases obtained in refs. [30–33] in simulations of confined Gay-Berne systems; it now

appears that the tilts seen in these systems were simply the entropically favoured arrangements for the surface potential employed, and were *not* caused by competition between particle-particle and particle-wall enthalpic contributions. The steric argument presented here is also consistent with the change from tilted to planar surface alignment observed when Wall and Cleaver [21, 31] simulated equivalent systems but with the molecular elongation reduced from $k = 3$ to $k = 2$; we now see that in the latter case, the particles were simply too short to significantly absorb at the surface and, therefore, adopted the planar state. Evaluation of $V_{\rm abs}(k = 2, \theta)$ (see Fig. 7) confirms this, showing that for this elongation, the absorbed volume is virtually independent of molecular orientation. In the light of this, it seems reasonable to assume that a planar surface arrangement would have been obtained in the simulations of Refs. [30–33], had the surfaces been represented by a lattice of fixed spheres, as was done in [23].

Thus, we conclude that for the HGO-sphere surface potential, a previously unrecognised angle-dependent absorption of particles into the surface leads to the formation of tilted phases, even for full particles. The anchoring behaviour obtained with this model is found to vary continuously with k_S/k, such that no bistability is found between the homeotropic and tilted anchoring states. That said, varying k_S/k does not appear to be the best route by which to control the anchoring tilt angle: changing the surface-sphere radius (σ_j in eqn.(3)) is a more natural approach to adopt. In the next Section, we address the behaviour induced by an alternative potential for which no such absorption can occur, the aim being to regain the standard homeotropic-planar anchoring behaviour obtained with the HNW potential.

III. THE HGO-SURFACE POTENTIAL

In this Section, we consider the behaviour of the HGO fluid when confined by a *full* (but structureless) substrate using the HGO-surface shape parameter derived in Appendix B, that is:

$$\sigma_w^{\rm HGO-surface} = \sigma_0 \left(\sqrt{\frac{1 - \chi_S \sin^2\theta}{1 - \chi_S}} - \frac{1}{2} \right). \qquad (7)$$

With this potential, each HGO particle effectively interacts with a planar continuum rather than a single sphere. Again a shift of $\sigma_0/2$ has been introduced so as to displace the material forming the substrate from the simulation box.

Before presenting the simulation results obtained for this system, we first consider the surface absorption properties expected for the modified shape parameter (7). Again, this is done by using the shape parameter to calculate $V_{\rm abs}(k, k_S, \theta)$ the particle volume absorbed into the surface as a function of its orientation and inner-particle extension. The results of this calculation for

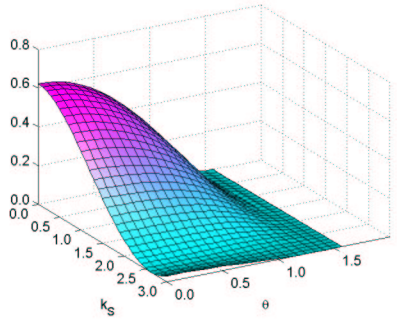

FIG. 8: [Color online] Representation of $V_{\rm abs}(k_s, \theta)$ for the HGO-surface potential and $k = 3$.

$k = 3$ are shown in Figure 8. From this we see that when $k_S = 0$, $V_{\rm abs}(k, k_S, \theta)$ is maximal at $\theta = 0$, indicating a stable homeotropic state. For $k_S = k = 3$, in contrast, $V_{\rm abs}(k, k_S, \theta)$ is close to zero for all θ, with only a small maximum present at $\theta = 0$. This maximum is, in fact, an anomaly relating to the ellipsoidal approximation employed in Appendix A; by design, $\sigma_w^{\rm HGO-surface}$ actually forbids any particle adsorption into the substrate if $k_S = k$. For this system, therefore, we expect to regain the planar base state previously found for rod-shaped objects in contact with a hard flat surface [18].

From these calculations, it is apparent that the mechanism driving any homeotropic-planar anchoring transition with the HGO-surface potential must be qualitatively different from that seen with the HNW potential [20]. For the latter, the stable anchoring state could be predicted by simply comparing the particle volume that could be absorbed into the surfaces in the homeotropic and planar arrangements: the favourable state was always that which maximized the total absorbed volume. In the case of the HGO-surface potential, however, there is *no* absorption in the planar arrangement. Here, therefore, the competition is between the higher orientational entropy of the planar state and the volume adsorption available (for $k_S < k$) in the homeotropic state.

A. Simulation results

The anchoring behaviour of the rod-surface potential has been studied using Monte Carlo simulations broadly equivalent to those presented in Section II A. All of the simulations were performed in the canonical ensemble on systems of $N = 1000$ HGO particles with elongation $k = 3$, confined in slab geometry with symmetric anchoring conditions. At each density investigated, two series of simulations were performed with increasing and decreasing k_S. The typical z-profiles for this model are shown in Figs. 9 and 10 for $k_S = 0.0$ and $k_S = k$, respectively.

The results obtained for $k_S = 0$ are virtually indistinguishable from those found for the equivalent HGO-

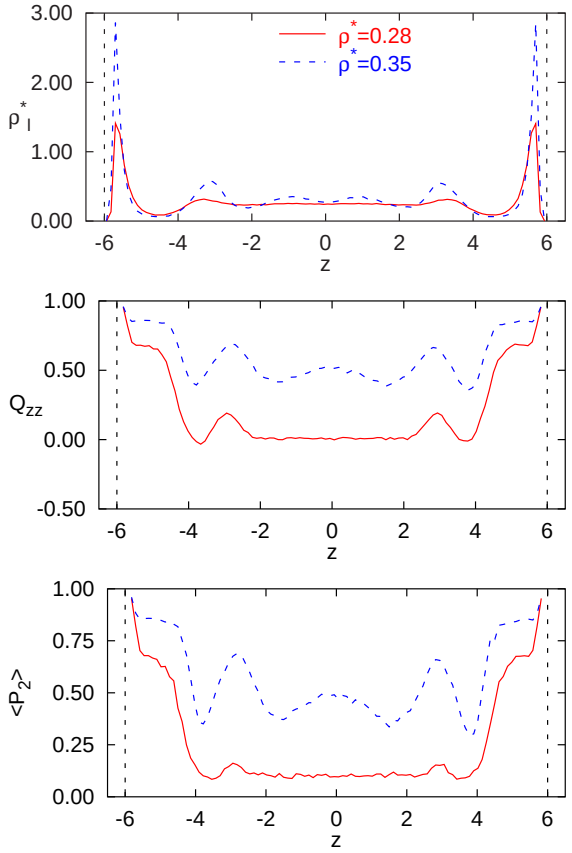

FIG. 9: [Color online] Typical z-profiles for systems of $N = 1000$ HGO particles with $k = 3.0$ and $k_S/k = 0.0$ confined using the HGO-surface potential. These data were obtained from a simulation series performed with decreasing k_S.

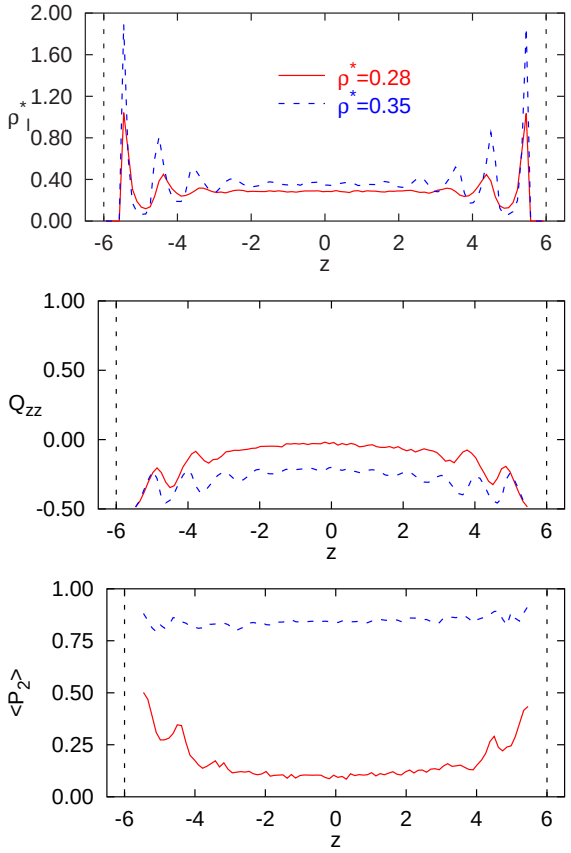

FIG. 10: [Color online] Typical z-profiles for systems of $N = 1000$ HGO particles with $k = 3.0$ and $k_S/k = 1.0$ confined using the HGO-surface potential. These data were obtained from a simulation series performed with decreasing k_S.

sphere system (recall Fig. 1), indicating, as expected, strong homeotropic anchoring. This similarity between the profiles obtained with the two $k_S = 0$ systems is explained by the observation that for $\alpha \simeq 0$, the interfacial geometry is equivalent for both potentials used. No such similarity is apparent for the two $k_S = k$ systems, however. Here, the HGO-surface system develops a multi-peak density profile with peak separations of σ_0, and, at nematic densities, a central region with negative $Q_{zz}(z)$ values. As predicted, therefore, this system does indeed adopt a planar state at high inner-particle elongation.

The full anchoring behaviour of this $k = 3$ system, evaluated as a function of k_S and ρ^*, is indicated by the anchoring maps shown in Figure 11. As previously, these show contours of $\overline{Q_{zz}}(\rho^*, k_S/k)$, the density-profile-weighted averages of $Q_{zz}(z)$ in the interfacial and bulk regions. Again, in calculating these, the surface region was taken to extend from the substrate to the second maximum in ρ^*_ℓ, regardless of the surface arrangement obtained. The anchoring maps computed for simulation series performed with decreasing and increasing k_S are given in Figs. 11(a) and (b), respectively. Clear differences are apparent from these two data sets, indicating hysteresis in the anchoring behaviour. This is quantified in the accompanying bistability maps (Figs. 11(c)) obtained by simply subtracting the (b) surfaces from their corresponding (a) surfaces. We note that the bistability indicated here covers a much wider range of both density and k_S/k than that obtained using the HNW potential [20], and is centred on $k_S/k \simeq 0.75$.

IV. CONCLUSIONS

We have investigated, by means of Monte Carlo computer simulation, the effect of the particle-substrate shape parameter (or contact function) on the anchoring behaviour of a generic confined liquid crystal model. Essentially, by tuning the degree and sense of the non-additivity of this contact function, we have been able to establish both a tilted anchoring state and a strongly first-order (i.e. bistable) planar to homeotropic anchoring transition.

Non-additivity has been incorporated into the systems studied in two different ways. Firstly, as was shown in Section II, the HGO-sphere shape parameter has an

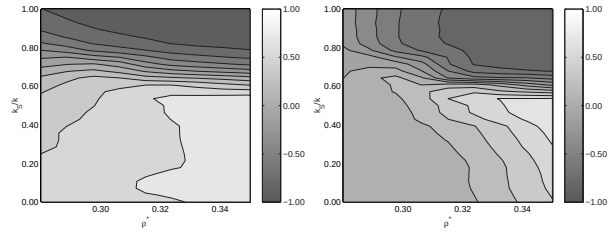

(a) Simulation series performed at constant density with decreasing k_S

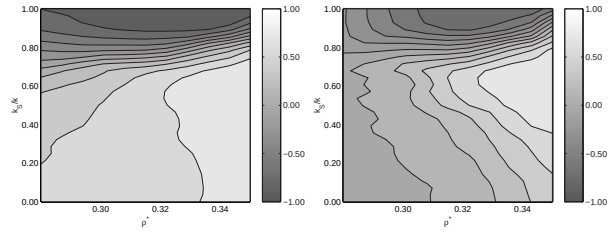

(b) Simulation series performed at constant density with increasing k_S

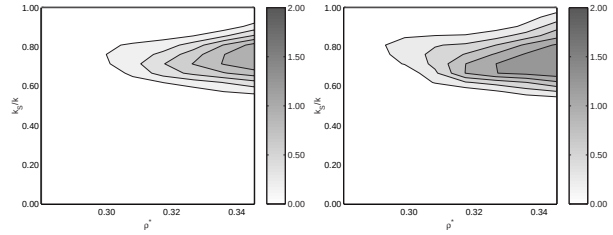

(c) Bistability maps obtained by subtracting Figs.(b) from Figs.(a)

FIG. 11: Anchoring maps obtained from simulations of $N = 1000$ $k = 3$ HGO particles confined using the HGO-surface surface potential. Diagrams on the l.h.s correspond to the interfacial region and those on the r.h.s correspond to the bulk region.

intrinsic angle-dependent non-additivity; particles approaching the substrate in either planar or homeotropic alignments 'see' the full surface, whereas particles approaching at intermediate angles are allowed to partially absorb. For systems with $k_S \approx k$, this microscopic effect was found to control both the structure of the fluid in the near-substrate region *and* the macroscopic anchoring orientation. The second use of non-additivity in this work centred on k_S, the (dimensionless) particle length used to determine the particle-substrate interactions. By using k_S as a model parameter, we have been able controllably to introduce a homeotropic anchoring state into the simulated systems, and continuously vary its relative stability. Given that particle shape is the main determinant of structure in most liquids, it should not, perhaps, be a great surprise that the contact function used to define particle-substrate interactions has had so dominant an effect here. That said, the utility of this approach does not appear to be widely recognised.

Whilst non-additivity has been used here as a convenient device with which to control model systems, we stress that this approach does not represent an abstract concept with no relevance to real systems. Indeed, for molecular systems (in which intramolecular flexibility may be significant) adsorbed at substrates with 'soft' coatings, the relevance of a fully-additive generic model is arguable. For the specific models used in this work, an experimental realisation of reducing the parameter k_S would be to employ a substrate coating that allows some penetration by the molecular endgroups, but repels the central part of the molecule; for mesogens, which commonly have sub-molecular units with significantly different character, this is perfectly achievable behaviour.

We have shown that the anchoring properties of generic model mesogens adsorbed at perfectly flat walls can be controlled by details of the mesogen-substrate interaction. Moreover, we have shown that the nature of the interfacial region can depend markedly on the anchoring state. For example, the depth at which the substrate profile ceases to be apparent in the liquid structure depends strongly on the anchoring orientation; since interfacial region structure underlies mesoscopic descriptors such as anchoring coefficients and surface viscosities, a more detailed understanding of such differences may offer a route to enhanced device control. Similarly, orientational correlations parallel with and perpendicular to the substrate can be expected to depend on the anchoring orientation; the systems determined here therefore represent good candidate systems with which to explore phenomena such as nematic bridging in microconfined and/or colloid-bearing mesogenic systems.

Finally, having achieved a microscopic model capable of exhibiting anchoring bistability, we are now in a position to examine the orientational behaviour present in more complex systems. These include other liquid crystal cell configurations, such as the bistable hybrid aligned nematic considered by Davidson and Mottram [6], and more exotic liquid crystal models such the PHGO description of flexoelectric pear-shaped particles [43].

Acknowledgments

FB wishes to acknowledge useful discussions with Dmytro Antipov and Sheffield Hallam University's Material Research Institute for financial support

APPENDIX A: VOLUME OF AN ELLIPSOID ABSORBED AT A PLANE

Here, we consider the geometry of an ellipsoidal particle close to a confining surface and interacting with it us-

ing an arbitrary potential that allows partial absorption into the substrate. The aim is to determine an expression for $V_{\rm abs}$, the volume absorbed into the surface. To this end, we consider the setups shown in Fig. 12. The result is first quoted for the case of a sphere of radius a: the volume of the illustrated sphere which is absorbed into the surface is

$$V_s = \frac{\pi}{3}(a-d_1)^2(2a+d_1). \tag{A1}$$

As indicated in the Figure, this same solution can then be transformed to the case of an ellipsoid of elongation k simply by scaling space by a factor k along the ellipsoid's symmetry axis, $\hat{\mathbf{z}}$, thus $V_{\rm abs} = kV_s$. What is required, therefore, is an expression for V_s in terms of the ellipsoid's co-ordinates.

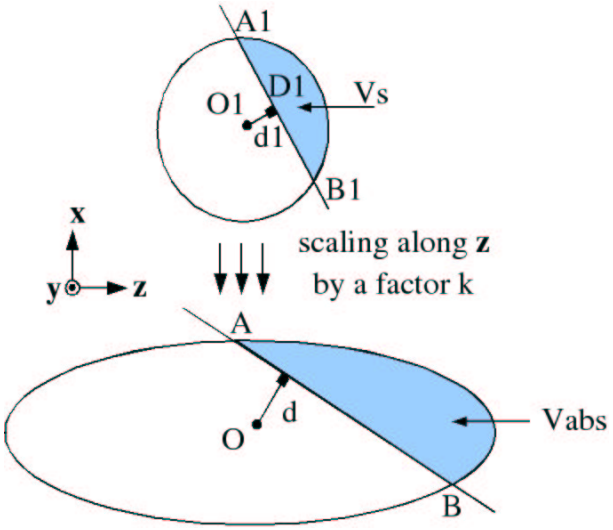

FIG. 12: [Color online] Schematic representation of the geometrical configuration considered in Appendix A to calculate the absorbed volume of an ellipsoid at a planar substrate.

The surface of an ellipsoid of semi-axes a, a, ka along $\hat{\mathbf{x}}, \hat{\mathbf{y}}$ and $\hat{\mathbf{z}}$ is given by

$$\frac{x^2}{a^2} + \frac{y^2}{a^2} + \frac{z^2}{k^2a^2} = 1. \tag{A2}$$

Taking the ellipsoid tilt to be confined to $\hat{\mathbf{x}}-\hat{\mathbf{z}}$ plane, the distance d_1 can be determined by considering the triangle OA_1B_1 in that plane. The co-ordinates of A_1 and B_1 are equal, respectively, to those of A and B rescaled by $1/k$ along $\hat{\mathbf{z}}$. Hence

$$\begin{aligned} A_1 &= \left(x_A, 0, \frac{z_A}{k}\right) \\ B_1 &= \left(x_B, 0, \frac{z_B}{k}\right) \end{aligned}$$

and, from Pythagoras' theorem,

$$d_1 = \sqrt{a^2 - \frac{1}{4}\left((x_A-x_B)^2 + \frac{1}{k^2}(z_A-z_B)^2\right)}. \tag{A3}$$

A and B, defined as the points in the $\hat{\mathbf{x}}-\hat{\mathbf{z}}$ plane where the ellipsoid intersects the substrate, can be found by solving the simultaneous equations

$$x^2 + \left(\frac{z}{k}\right)^2 = a^2 \tag{A4}$$

$$x\sin\theta = z\cos\theta - d. \tag{A5}$$

Combining these gives

$$z^2\left(k^2\cos^2\theta + \sin^2\theta\right) - 2zk^2 d\cos\theta + d^2k^2 - a^2k^2\sin^2\theta = 0 \tag{A6}$$

the roots of which are

$$z = \frac{dk^2\cos\theta \pm \sqrt{k^2\sin^2\theta\left[a^2(k^2\cos^2\theta+\sin^2\theta) - d^2\right]}}{k^2\cos^2\theta + \sin^2\theta}. \tag{A7}$$

Eqn. (A3) can now be rewritten using

$$\begin{aligned} (x_B - x_A)^2 &= \frac{\cos^2\theta}{\sin^2\theta}(z_B - z_A)^2 \\ (z_B - z_A)^2 &= \frac{4k^2\sin^2\theta\left[-d^2 + a^2\left(k^2\cos^2\theta + \sin^2\theta\right)\right]}{(k^2\cos^2\theta+\sin^2\theta)^2} \end{aligned}$$

which, after full simplification, reduces to

$$d_1 = \frac{d}{\sqrt{k^2\cos^2\theta + \sin^2\theta}}. \tag{A8}$$

Having obtained this expression for d_1 purely in terms of the ellipsoid co-ordinates, we insert it into eqn. (A1) and scale by k to give the absorbed volume of the ellipsoid

$$V_{\rm abs}(k,\theta) = \frac{k\pi}{3}\left(a - \frac{d}{\sqrt{k^2\cos^2\theta+\sin^2\theta}}\right)^2 \times \left(2a + \frac{d}{\sqrt{k^2\cos^2\theta+\sin^2\theta}}\right). \tag{A9}$$

APPENDIX B: DETERMINATION OF THE ROD-SURFACE $\sigma_w^{\rm HGO-surface}$

In this appendix, we give two routes to the rod-surface shape parameter employed in Section III of this paper. The first approach adopted here is to take the Gaussian-overlap (GO) rod-sphere interaction given by Berne and Pechukas [35] and integrate the position of the sphere across the xy-plane. The result of this calculation is then compared with the generic GO form to allow identification of a rod-surface shape parameter, $\sigma(\theta)$. In the second approach, this same result is obtained by direct calculation of the minimum distance between a single GO particle and a sphere constrained to lie in the surface plane.

As a starting point, we take eqn.(4) of [35], the GO interaction potential for two ellipsoidal particles:

$$V(\hat{\mathbf{u}}_i, \hat{\mathbf{u}}_j, \mathbf{r}_{ij}) = \varepsilon(\hat{\mathbf{u}}_i, \hat{\mathbf{u}}_j)\exp\left[-\frac{r_{ij}^2}{\sigma^2(\hat{\mathbf{u}}_i, \hat{\mathbf{u}}_j, \hat{\mathbf{r}}_{ij})}\right] \tag{B1}$$

When one of the particles is made spherical, to give a rod-sphere interaction, Berne and Pechukas tell us that the shape parameter becomes

$$\sigma(\hat{\mathbf{u}}_i, \hat{\mathbf{r}}_{ij}) = \sqrt{\frac{\sigma_0^2 + \sigma_j^2}{2(1 - \chi(\hat{\mathbf{u}}_i \cdot \hat{\mathbf{r}}_{ij})^2)}} \tag{B2}$$

where

$$\chi = \frac{\sigma_\ell^2 - \sigma_0^2}{\sigma_\ell^2 + \sigma_j^2}. \tag{B3}$$

On inserting (B2) into (B1), the resultant interaction between a rod and a sphere is

$$V(\hat{\mathbf{u}}_i, \mathbf{r}_{ij}) = \varepsilon_0 \exp\left[-\frac{2r_{ij}^2\{1 - \chi(\hat{\mathbf{u}}_i \cdot \hat{\mathbf{r}}_{ij})^2\}}{\sigma_0^2 + \sigma_j^2}\right]. \tag{B4}$$

With the aim of extending this to calculate a rod-surface interaction, we take eqn. (B4) and integrate the sphere's position over the xy-plane. To do this, we define a coordinate system such that $\hat{\mathbf{u}}_i = (\sin\theta, 0, \cos\theta)$ and $\mathbf{r}_{ij} = (x, y, z)$. With these definitions (and redefining ε to have units of energy per unit area), the double integral over $V(\hat{\mathbf{u}}_i, \mathbf{r}_{ij})$ becomes

$$V(\hat{\mathbf{u}}_i, z) = \varepsilon_0 \int\int_{\mathrm{xy-plane}} \exp\left[-\frac{2(x^2 + y^2 + z^2 - \chi(x\sin\theta + z\cos\theta)^2)}{\sigma_0^2 + \sigma_j^2}\right] dxdy \tag{B5}$$

The y-integral is a straightforward Gaussian, and the x-integral is just a 'complete the square' problem. Performing these gives

$$V(\hat{\mathbf{u}}_i, z) = \varepsilon_0 \exp\left[-\frac{2z^2(1 - \chi)}{(\sigma_0^2 + \sigma_j^2)(1 - \chi\sin^2\theta)}\right]. \tag{B6}$$

Comparing this with the generic GO form (i.e. eqn. (B1)), we can identify $\sigma(\theta)$ with the square root of the terms dividing z^2 in the exponential term in eqn. (B6). So, the final result is

$$\sigma(\theta) = \sqrt{\frac{(\sigma_0^2 + \sigma_j^2)(1 - \chi\sin^2\theta)}{2(1 - \chi)}} = \sigma_0\sqrt{\frac{1 - \chi\sin^2\theta}{(1 - \chi)}} \tag{B7}$$

where the second equality requires the (usual) imposition $\sigma_0 = \sigma_j$.

Interestingly, the result (B7) obtained by integrating over the gaussian containing the rod-sphere shape parameter can alternatively be obtained in a process involving differentiation of that same rod-sphere shape parameter. To see this, we consider an HGO particle located in the vicinity of a planar interface and seek to calculate the distance between the interface and the closest part of the rod. Taking the rod-sphere shape parameter to define the shape of the rod as viewed by the interface, what this then amounts to is identifying the sphere, constrained to lie in the plane, whose location minimises the shape parameter calculation.

The $\mathbf{r}_{ij}$ vector corresponding to this minimum can be identified simply by differentiating an expression for the projection of $\hat{\mathbf{r}}_{ij}\sigma(\hat{\mathbf{u}}_i, \hat{\mathbf{r}}_{ij})$ along the surface normal and setting it to zero. For arbitrary $\hat{\mathbf{r}}_{ij}$, this projection is given by

$$\sigma_z(\hat{\mathbf{u}}_i, \hat{\mathbf{r}}_{ij}) = (\hat{\mathbf{r}}_{ij} \cdot \hat{\mathbf{z}})\sqrt{\frac{\sigma_0^2 + \sigma_j^2}{2(1 - \chi(\hat{\mathbf{u}}_i \cdot \hat{\mathbf{r}}_{ij})^2)}}. \tag{B8}$$

Writing $\hat{\mathbf{r}}_{ij} = (\sin\phi, 0, \cos\phi)$ the turning points of (B8) are given by

$$\tan(\phi_{\min}) = \frac{\chi\cos\theta\sin\theta}{1 - \chi\sin^2\theta}. \tag{B9}$$

This gives the orientation of $\hat{\mathbf{r}}_{ij}$ corresponding to the point on the rod that is nearest to the surface. Using (B9) to substitute for ϕ in (B8) and performing some trigonometrical manipulation then gives an expression for $\sigma(\theta)$ which is identical to that given by (B7).

[1] B. Jérôme, Phys. Rep. **54**, 391 (1991).
[2] I.A. Shanks, Contemp. Phys. **23**, 65 (1982).
[3] T. Geelhaar, Liq. Crysts. **24**, 91 (1998).
[4] G.P. Bryan-Brown, C.V. Brown, I.C. Sage and V.C. Hui, Nature **392**, 365 (1998).
[5] C. Denniston and J.M. Yeomans, Phys. Rev. E **87**, 275505 (2001).
[6] A.J Davidson and N.J. Mottram, Phys. Rev. E **65**, 051710 (2002).
[7] B. Tjipto-Margo and D.E. Sullivan, J. Chem. Phys. **88**, 6620 (1988).
[8] E. Martín del Río, M.M Telo da Gama and E. de Miguel, Phys. Rev. E **52**, 5028 (1995).
[9] M.A. Osipov and S. Hess, J. Chem. Phys. **99**, 4181 (1993).
[10] P.I.C Teixeira, Phys. Rev. E **55**, 2876 (1997).
[11] M.P. Allen, Molec. Phys. **96**, 1391 (1999).
[12] Z. Lu, H. Deng and Y. Wei, Supramol. Sci. **5**, 649 (1998).
[13] W. Chen, M.B. Feller and Y.R. Shen, Phys. Rev. Letts. **63**, 2665 (1989).
[14] N.A. Clark, Phys. Rev. Letts. **55**, 292 (1985).
[15] J.M. Geary, J.W. Goodgy, A.R. Kmetz and J.S. Patel, J. Appl. Phys. **62**, 4100 (1987).
[16] D.W. Bereman, Phys. Rev. Letts. **28**, 1683 (1972).
[17] R. van Roij, M. Dijkstra and R. Evans, Europhys. Letts. **49**, 350 (2000).

[18] M. Dijkstra, R. van Roij and R. Evans, Phys. Rev. E **63**, 051703 (2001).
[19] A. Chrzanowska, P.I.C. Teixeira, H. Ehrentraut and D.J. Cleaver, J. Phys.: Cond. Matt. **13**, 4715 (2001).
[20] F. Barmes and D.J. Cleaver, Phys. Rev. E **69**, 061705 (2004).
[21] G.D. Wall and D.J. Cleaver, Molec. Phys. **101**, 1105 (2003).
[22] D.R. Binger and S. Hanna, Liq. Crysts. **28**, 1215 (2001).
[23] V. Palermo, F. Biscarini and C. Zannoni, Phys. Rev. E **57**, R2519 (1998).
[24] D.J. Cleaver and P.I.C Teixeira, Chem. Phys. Letts. **338**, 1 (2001).
[25] H. Lange and F. Schmid, J. Chem. Phys. **111**, 362 (2002).
[26] H. Lange and F. Schmid, Euro. Phys. J. E **7**, 175 (2002).
[27] H. Lange and F. Schmid, Comp. Phys. Comms. **147**, 276 (2002).
[28] M.T. Downton and M.P. Allen, Europhys. Letts. **65**, 48 (2004).
[29] D. Antypov and D.J. Cleaver, J. Phys.: Cond. Matt. **16**, S1887 (2004).
[30] Z. Zhang, A. Chakrabarti, O.G. Mouristen and M.J. Zuckermann, Phys. Rev. E **53**, 2461 (1996).
[31] G.D. Wall and D.J. Cleaver, Phys. Rev. E **56**, 4306 (1997).
[32] P.I.C Teixeira, A. Chrzanowska, G.D. Wall and D.J. Cleaver, Molec. Phys. **99**, 889 (2001).
[33] R.E. Webster, N.J. Mottram and D.J. Cleaver, Phys. Rev. E **68**, 021706 (2003).
[34] M. Rigby, Molec. Phys. **68**, 687 (1989).
[35] B.J. Berne and P. Pechukas, J. Chem. Phys. **56**, 4213 (1972).
[36] J.G. Gay and B.J. Berne, J. Chem. Phys. **74**, 3316 (1981).
[37] P. Padilla and E. Velasco, J. Chem. Phys. **106**, 10299 (1997).
[38] E. de Miguel, E. Martín del Río, J. Chem. Phys. **115**, 9072 (2001).
[39] E. de Miguel, E. Martín del Río, J. Chem. Phys. **118**, 1852 (2003).
[40] E. de Miguel, Phys. Rev. E **47**, 3334 (1992).
[41] N.V. Priezjev, G. Skačej, R.A. Pelkovits and S. Žumer, Phys. Rev. E **68**, 041709 (2003).
[42] F. Barmes and D.J. Cleaver, in preparation (2004).
[43] F. Barmes, M. Ricci, C. Zannoni and D.J. Cleaver, Phys. Rev. E **68**, 021708 (2003).